JOURNAL OF THEORETICAL
AND APPLIED MECHANICS
https://doi.org/10.15632/jtam-pl/204804
ONLINE FIRST

INVESTIGATION INTO RESISTANCE FORCES FROM THE WHEEL-RAIL INTERFACE OF A FOUR-AXLE RAILWAY VEHICLE IN CURVED TRACK

Máté M. SZŰCS*, Zoltán ZÁBORI

Department of Railway Vehicles and Vehicle System Analysis, Budapest University of Technology and Economics, Budapest, Hungary

*corresponding author, *m.szucs.mate@kjk.bme.hu*

This study focuses on the resistance forces resulting from the wheel-rail contact in a four-axle railway vehicle operating on curved tracks of varying radii and quality. Using a dynamic simulation tool, the research analysed over 900 simulations to compute energy dissipation and specific resistance forces. The findings reveal that curve resistance decreases with larger curve radii, whereas deteriorating track quality leads to higher resistance and increased deviation. The results emphasize the significant impact of track quality on resistance forces, particularly for larger curve radii. Future research aims to refine regression models and explore the deviation reduction in resistance for small-radius curves.

Keywords: wheel-rail contact; energy dissipation; resistance force; curve resistance force; dynamical simulation.

1. Introduction

Resistance forces are important to consider in the design and operation of rail vehicles and need to be studied in more depth for several reasons. Determining resistance forces is relevant for predicting wheel and rail wear, for using longitudinal dynamic models, for obtaining the maximum hauled train load, for simulating the energy consumption of train movements (Garg & Dukkipati, 1984; Jerrelind *et al.*, 2021). The main part of resistance forces is the force resulting from the inevitable loss of energy due to the wheel-rail rolling contact (Tkachenko *et al.*, 2016). In general, this loss is difficult to estimate because multiple parameters are involved, and this process becomes more complex considering movements on curved track sections. Resistance forces in curves remain a significant research area today, both with simulation and experimental approaches (Michálek *et al.*, 2024; Semenov *et al.*, 2023; Wu *et al.*, 2020).

The lateral movement of the vehicle on the track has a strong influence on the energy loss. Due to lateral track irregularities, the lateral displacement impacted of the vehicle; the track quality therefore influences the resistance forces (Iwnicki *et al.*, 2015; Tunna & Urban, 2009). However, previous studies have not comprehensively examined this phenomenon in terms of resistance forces.

This paper is the investigation of energy dissipation from wheel-rail contact based on dynamic simulation of curved track sections and different specifications with stochastic lateral track irregularities and their comparative analysis.

The publication has been funded by the Polish Ministry of Science and Higher Education under the Excellent Science II programme "Support for scientific conferences".
The content of this article was presented during the 40th Danubia-Adria Symposium on Advances in Experimental Mechanics, Gdańsk, Poland, September 24–27, 2024.

2. Computation method

The computational method is based on simulation using a lateral dynamic model of a four-axle, two-bogie railway vehicle in the excited lateral dynamics in arbitrary curving and the wear (ELDACW) program system developed by the Department of Railway Vehicles and Vehicle System Analysis (TU Budapest) (Szabó *et al.*, 1994). The program system was specifically designed for the investigation of dynamic interaction between the wheel and rail interface, thereby enabling a detailed analysis of the resistance forces arising from the wheel-rail contact (Zobory, 1997).

Figure 1 illustrates the flowchart of the calculation method. By simulating the vehicle motion, the dissipated power $W(t)$ from the wheel-rail contact is calculated over time t:

$$W(t) = \int_0^t P(\tau)\,\mathrm{d}\tau, \tag{2.1}$$

where P is the power dissipated in wheel-rail contact, with the time variable τ.

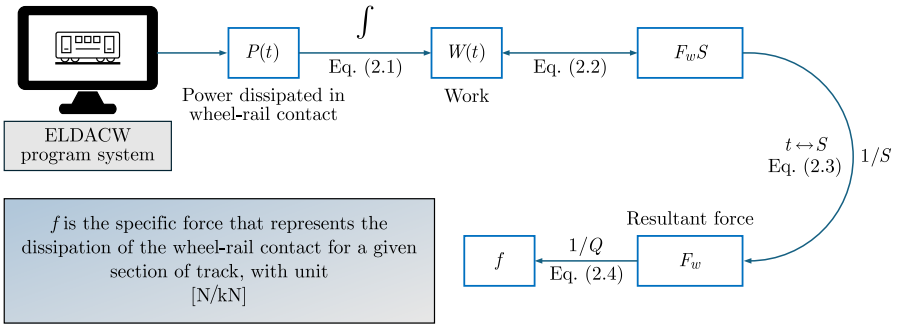

Fig. 1. Flowchart of the calculation method.

A force of constant magnitude can be defined that does the same work W on a given section of road:

$$W(t) = \int_0^S F_w^*(s)\,\mathrm{d}s = \int_0^t P(\tau)\,\mathrm{d}\tau = F_W S, \tag{2.2}$$

where $F_w^*(s)$ is the resultant force at the wheel-rail contact of the variable magnitude for a given section of track, depending on the travelled distance s, F_W is the force of constant magnitude associated with the total travelled distance S, with a work equal to the work $W(t)$. The resistance force calculated from the loss of wheel-rail contact on a given section of track can be determined by the following formula:

$$F_W = \frac{W(t)}{S}. \tag{2.3}$$

Dividing the resistance force in Eq. (2.3) by the vehicle's weight Q gives the specific drag force per unit weight, in [N/kN]:

$$f = \frac{1}{Q} F_W = \frac{\displaystyle\int_0^S F_w^*(s)\,\mathrm{d}s}{SQ}. \tag{2.4}$$

The specific resistance force f in expression (2.4) is used to describe the loss due to wheel-rail contact for the vehicle on a given section of track. It depends on the vehicle's motion whether

the specific resistance force f is nearly constant after a distance. If the distance is too short, the result may be unreliable; the value may refer to a particular section of track or to the transient motion of the vehicle, while if the distance is too long, the computational requirements of the simulations increase (M. Szűcs, 2024).

3. Dynamical model

The complete vehicle-track dynamic model incorporates a total of 34 degrees of freedom (DoFs). These include the vehicle body, two bogie frames, two bogie bolsters, four wheels, and the equivalent track-masses placed under the individual wheels to represent the inertia of the track. Each of these components is modelled as a rigid mass. The main features of the model are:

- all rigid bodies, except for the equivalent track-masses, possess lateral displacement, and rotation around the vertical (z) axis (yaw movement) (2 DoFs $\times$ 9 components). The wheelsets have two additional DoFs: rotation around their own axes and longitudinal displacement. These are necessary to include in the model for calculating creep forces (2 DoFs $\times$ 4 wheelsets). The 8 equivalent track-masses have lateral displacement, allowing the representation of track flexibility in the lateral direction (1 DoF $\times$ 8 components). The total DoFs of the model is 34;
- the program system incorporates equations corresponding to all degrees of freedom of the rigid bodies, based on Newton's second law applied to acceleration and momentum, used for translational and rotational movement;
- the lateral deviations of rails from their nominal position, in the form of track-unevenness functions can be taken into consideration;
- the wheel-rail force at the wheel tread is modelled as a creep-dependent force, where the relationship between creep and the friction coefficient is nonlinear (Zobory, 2008);
- the flange contact is considered as a lateral, linearly elastic, and damped connection linking the wheel to the mass representing the track in the case where the contact point is on the wheel flange.

In the simulation, the parameters of a reference UIC Z passenger car were considered for modelling the four-axle rail vehicle. Table 1 contains the main characteristics of the standard gauge passenger car, and the vehicle model is shown in Fig. 2.

Table 1. Main characteristic of the passenger car.

Maximum speed of the vehicle during the simulation	120	km/h
Mass of vehicle body (m_{sz})	34800	kg
Mass of bogie (m_f)	3800	kg
Mass of wheelset (m_k)	1600	kg
Mass of bolster (m_h)	200	kg
Yaw inertia of the vehicle body (Θ_{sz})	20 000 000	$\mathrm{kg \cdot m^2}$
Yaw inertia of the bogie (Θ_f)	4500	$\mathrm{kg \cdot m^2}$
Pitch inertia of the wheelset (Θ_{ky})	110	$\mathrm{kg \cdot m^2}$
Yaw inertia of the wheelset (Θ_{kz})	820	$\mathrm{kg \cdot m^2}$
Yaw inertia of the bolster (Θ_h)	150	$\mathrm{kg \cdot m^2}$
Bogie centre base distance (l_f)	19	m
Bogie wheelbase (l_k)	2.5	m
Height of the centre of gravity of the vehicle body (h_s)	1.7	m
Friction torque on a wheelset axle	100	Nm
Wheel load – each wheel (Q)	60.09	kN

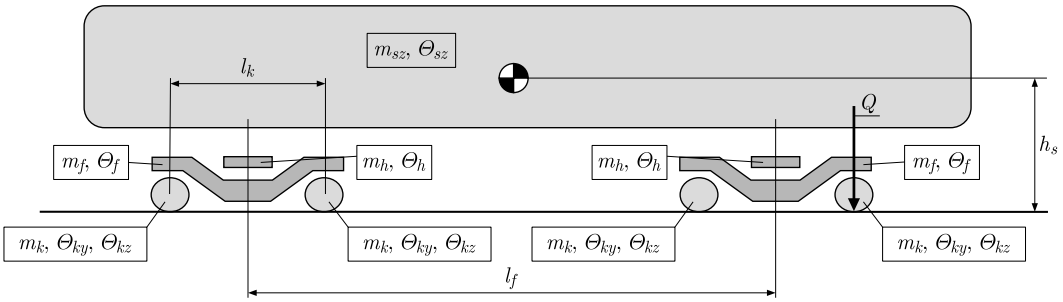

Fig. 2. Passenger car's main dimensions and masses.

4. The generation of track lateral irregularity

The lateral track irregularities are approximated by the realisation of a weakly stationary stochastic process defined along the track length. In this context, a stochastic process refers to a random function which has statistical properties (i.e., mean, deviance) remaining constant over space (i.e., along the track). The realisations are constructed using one-sided spectral density functions derived from measured data (Frederich, 1984). Simulations are conducted for three track quality levels: ideal (category I) without irregularities, good (category II), and medium (category III) from (Frederich, 1984).

The main track geometric parameters affecting the lateral position of the vehicle are track gauge and alignment. The deviations of the right and left rails from the geometric ideal are the combined effect of the track gauge and the alignment, which are generated by random number realisation generation (Szabó & Zobory, 1998). From the spectral density functions, 150–150 different realisations of each track category were generated for the simulation and used to define track irregularities in different curved track sections, with 75 m length. The total length of the track sections corresponding to the given curve and quality level is 11.25 km (M. Szűcs & Zábori, 2024).

Figure 3 illustrates the realisation of a typical category II lateral track irregularity for the right and left rails.

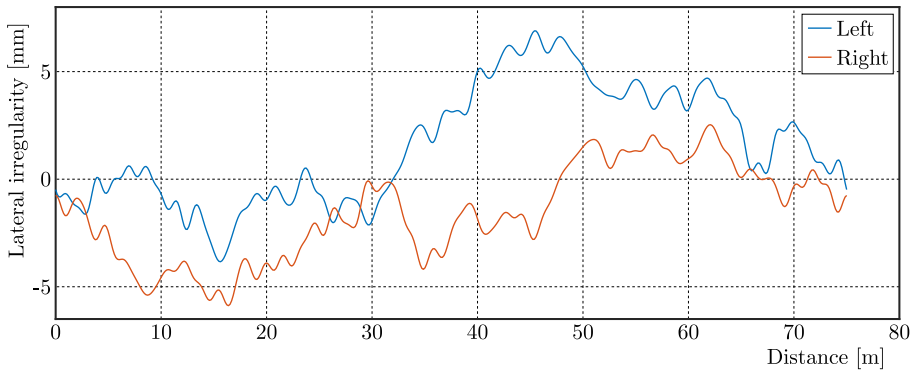

Fig. 3. Lateral track irregularity realisation.

The simulations were performed for six different curve radii in addition to the two quality categories mentioned above (category II and III) and for an ideal track without track irregularity (category I).

The initial values of the simulation are calculated in a preliminary step by ELDACW. To prevent computational errors in the approximate initial values from affecting the final simulation results, the summation of the dissipation from the wheel-rail contact was started after a certain distance travelled by the vehicle. Based on the preliminary simulation results, the length of this section used in the study is 40 % (30 m) of the 75 m base wavelength of the track irregularity.

5. Details of track lateral irregularity

The EN 13848 standard family (Railway applications – Track – Track geometry quality) recommends a wavelength range of 3–70 m for the geometric classification of railway tracks. Rail vehicle dynamics are usually evaluated at frequencies between 0.4 Hz and 20 Hz. The selected track irregularity has a base wavelength of 75 m and a minimum wavelength of 1.5 m. The frequency range for the maximum speed of 120 km/h is 0.44 Hz–22.22 Hz for wavelengths between 1.5 m–75 m. In curves with small radius, the speed needs to be limited, for lower speeds this range shifts to lower values.

The standard sets three different limits for different types of track defects, which are derived from experimentation/experience. These are the following:

– immediate action limit – IAL;
– intervention limit – IL;
– alert limit – AL.

The relation between them:

$$\text{IAL} > \text{IL} > \text{AL}. \tag{5.1}$$

The realisations of track gauges are mainly of zero mean value. In the category III, there may be realisations where the gauge narrowing is more than the value that still ensures the lateral positioning of the wheel without "locking" (−8.1 mm). Therefore, in these realisations, both rails are shifted "outwards" – the left rail to the left, the right rail to the right – symmetrically by a value that ensures that the track gauge error does not exceed −8.1 mm. This adjustment does not represent standard maintenance practice but rather serves as a computational strategy to ensure stability of the simulation. Importantly, all adjustments have been kept within the intervention limit (IL) thresholds specified in EN 13848, ensuring that our track geometry remains representative of acceptable real-world conditions. We have verified that this technical simplification does not meaningfully impact our results, as the primary dynamic interactions remain governed by the same physical principles.

The parameters of the tracks from categories II and III used for the simulations in relation to these limits are given in Table 2 in terms of track gauge and alignment, to compare to the values in the standard. Explanation of the rows in the table from the EN 13848 standard family:

– TG – ID: track gauge – AL/IL/IAL – isolated defects – nominal track gauge to peak value;
– TG – NTG: track gauge – AL/IL/IAL – nominal track gauge to mean track gauge (over 100 m);
– AM – ID: alignment – AL/IL/IAL – isolated defects – zero to a peak value (D1 3 m–25 m, D2 N/A);
– AM – SD: alignment – standard deviation – (wavelength 3 m–25 m).

Table 2. Parameters used for simulation of category II and III tracks compared to the limits of the EN 13848 standard family – minimum, maximum and expected values (EV).

	Limits in EN 13848 $80 < V$ [km/h] ≤ 120 [mm]	Category II [mm]	Category III [mm]
TG – ID	IL: MIN −9 | MAX +30	MIN −8.1 | MAX 6.6	MIN −8.1 | MAX 27.1
TG – NTG	AL: MIN −5 | MAX +16	MIN 0 | MAX 0	MIN 0 | MAX 13.4
AM – ID	IAL: MAX 17	EV 2.25 | MAX 4.26	EV 8.72 | MAX 16.52
AM – SD	Class from B to E	EV 0.93 | MAX 1.71	EV 3.51 | MAX 6.31

6. Results

The simulation results are shown in Table 3, for six different curve radii, categories I, II, and III.

Table 3. Simulation results.

Cases	$R = 300\,\mathrm{m}$	R400	R600	R900	R1500	R3000
	A	B	C	D	E	F
V [km/h]	60	80	100	120	120	120
h [mm]	80	128	136	128	52	56
τ [m/s^2]	0.40	0.40	0.40	0.40	0.40	0
I. f	1.90	1.41	1.01	0.71	0.37	0.10
II. f_{II}	1.92 +1 %	1.45 +3 %	1.00 −1 %	0.68 −4 %	0.42 +13 %	0.25 +144 %
III. f_{III}	2.00 +5 %	1.60 +14 %	1.27 +25 %	1.14 +59 %	1.06 +182 %	1.01 +897 %
II. d	0.00	0.01	0.01	0.01	0.02	0.03
d [%]	0	0	1	1	4	14
III. d	0.03	0.05	0.09	0.13	0.15	0.17
d [%]	2	3	7	12	15	17

In Table 3, V is the constant speed of the vehicle, h is the cant of the curve and τ is the unbalanced lateral acceleration. f is the value obtained on the ideal track in category I, and the expected value of the simulation is based on the realisation of 150 different realisations in categories II and III. The value d is calculated for each case and represents the standard deviation normalised to the given f in %.

For validation purposes, Table 4 presents a comparison between resistance forces derived from detailed theoretical formulations found in the literature and the results obtained for the ideal track (Schramm, 1963), clearly demonstrating the similarity between them.

Table 4. Simulation results of category I compared to literature values [N/kN].

Cases	A	B	C	D	E	F
I. f	1.90	1.41	1.01	0.71	0.37	0.10
Schramm $\dfrac{160 l_k + 162}{R}$	1.87	1.41	0.94	0.62	0.37	0.19

Based on Tables 3 and 4, it can be stated that the resistance forces decrease with increasing curve radius, in accordance with simulation (Wu *et al.*, 2020) and experimental (Lukaszewicz, 2008; Schmidt, 1927) results in the literature, and as derived from theoretical considerations. This trend is also found for categories II and III. However, the literature shows that the resistance forces calculated from empirical and theoretical formulas exhibit significant variability (Wu *et al.*, 2020).

In terms of track quality, it can be concluded that the lower the quality, the higher the resistance force. The difference increases for a larger curve radius compared to the ideal track. This phenomenon was also detected in simulations by (Bailey & Hedrick, 1988; Tunna & Urban, 2009) and the results align with the previous findings provided by the referred literature (Michálek *et al.*, 2024).

Figure 4 shows the standard deviation for categories II and III.

The standard deviation of the resistance values for each realisation shows a similar trend for both track qualities: a larger curve radius is associated with a larger standard deviation and hence a larger range. The results for the six curve radii are shown in Fig. 5.

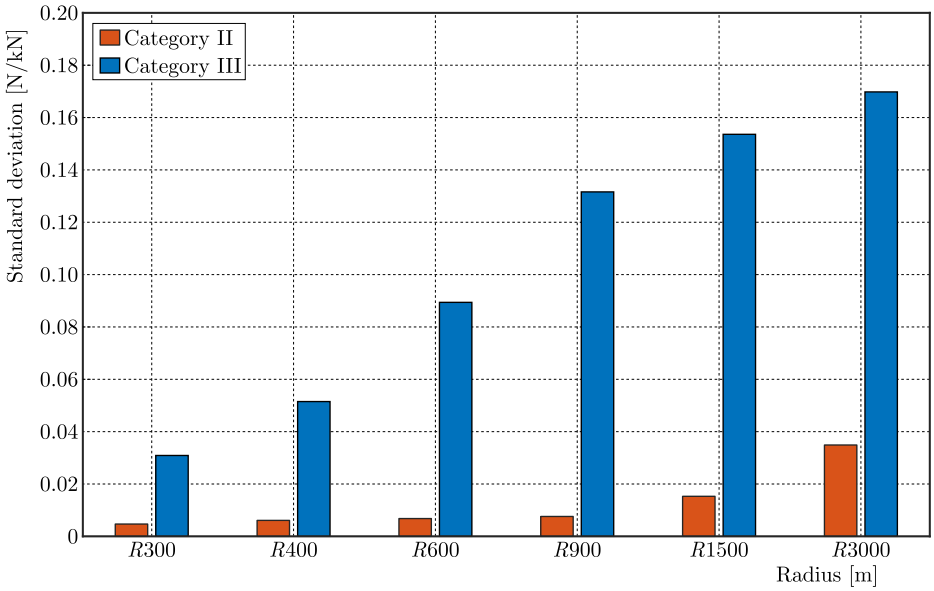

Fig. 4. Standard deviation of resistance forces for categories II and III.

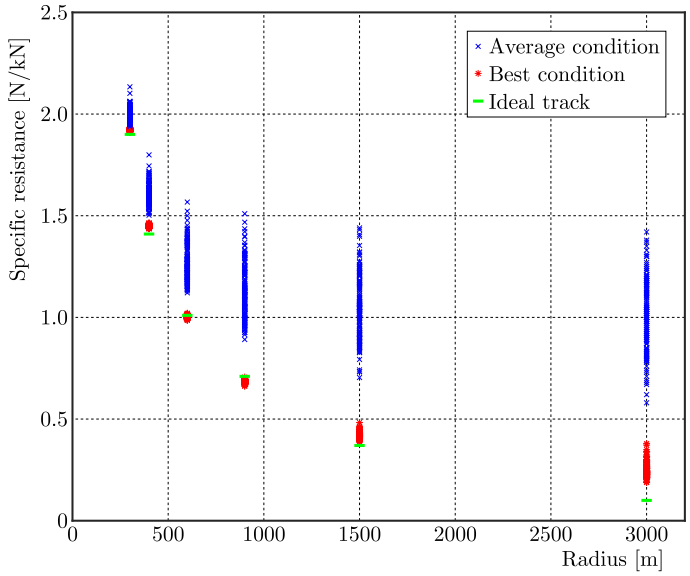

Fig. 5. Results for the six curve radii.

While for category II there is no overlap between the results for different curve radii, for category III the higher resistance forces overlap largely in the cases C to F for the adjacent curve radius. Thus, although the expected values are well separated in each curve (Table 3, f, f_{II}, and f_{III}), the resistive forces associated with each track section under stochastic track irregularity are loaded with great uncertainty.

In Fig. 6, beyond showing the expected values, we have included the 95% confidence intervals calculated using the t-distribution for each track quality category, which appropriately addresses the varying standard deviations and unknown distributions in our results. Simple linear connections between different curve radius points effectively illustrate how potential regression models would differ depending on track quality. Table 5 shows the lower and upper limits of categories II and III.

Figures 7 and 8 show the results for categories II and III, represented by boxplots and histograms (Danz, 2024). These figures illustrate the large difference in the range of values for categories II and III caused by the quality of the track. Compared to the expected values of

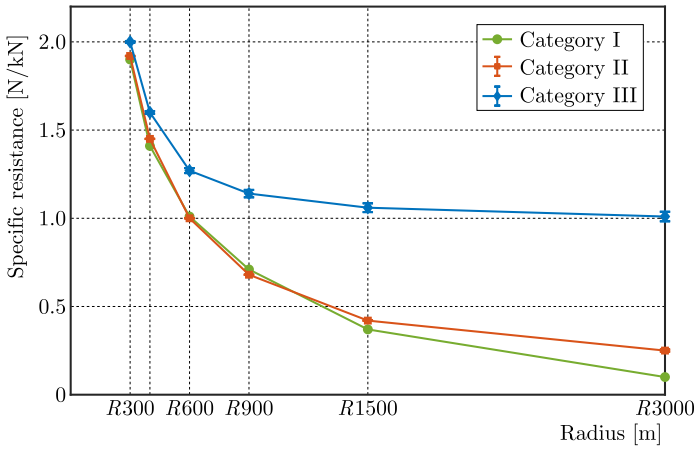

Fig. 6. 95 % confidence intervals calculated using t-distribution.

Table 5. 95 % confidence intervals calculated using t-distribution for categories II and III [N/kN].

Cases		A	B	C	D	E	F
II.	lower	1.919	1.449	0.999	0.679	0.418	0.244
	upper	1.921	1.451	1.001	0.681	0.422	0.256
III.	lower	1.995	1.592	1.256	1.119	1.035	0.983
	upper	2.005	1.608	1.284	1.161	1.085	1.037

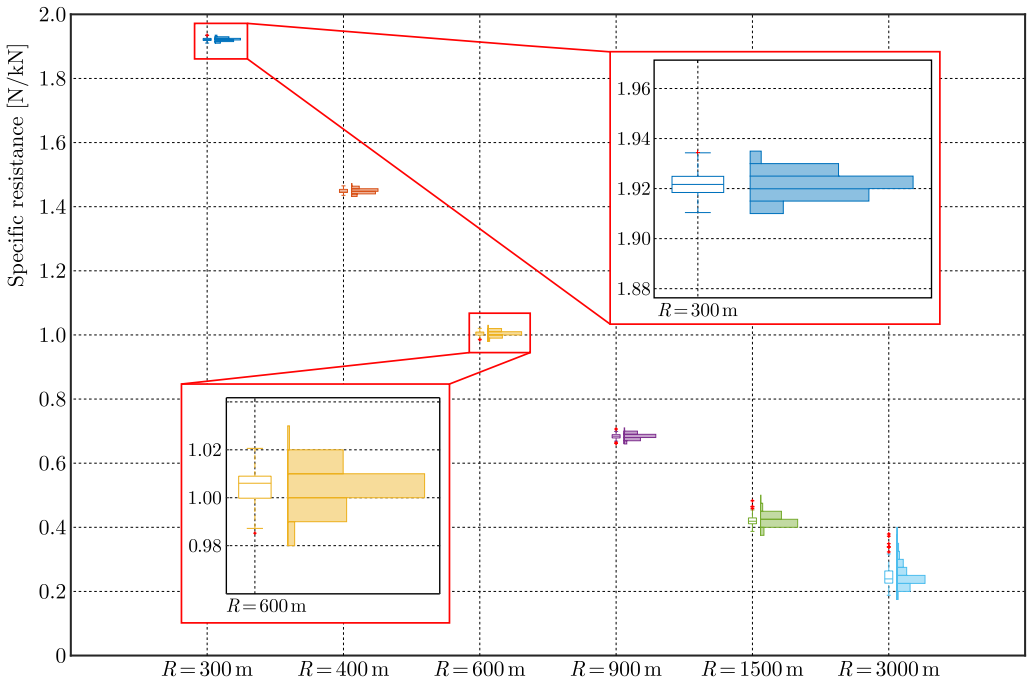

Fig. 7. Distribution of specific resistance values using boxplot and histogram, category II.

the specific resistances, the standard deviation is almost negligible for category II. Figure 6 shows the highlighted details of the 300 and 600 metre radii. In contrast, for category III with higher curve radii, the difference between the maximum and minimum values is comparable to the expected value. For larger curve radii and lower track quality, there is a large uncertainty in the resistance values.

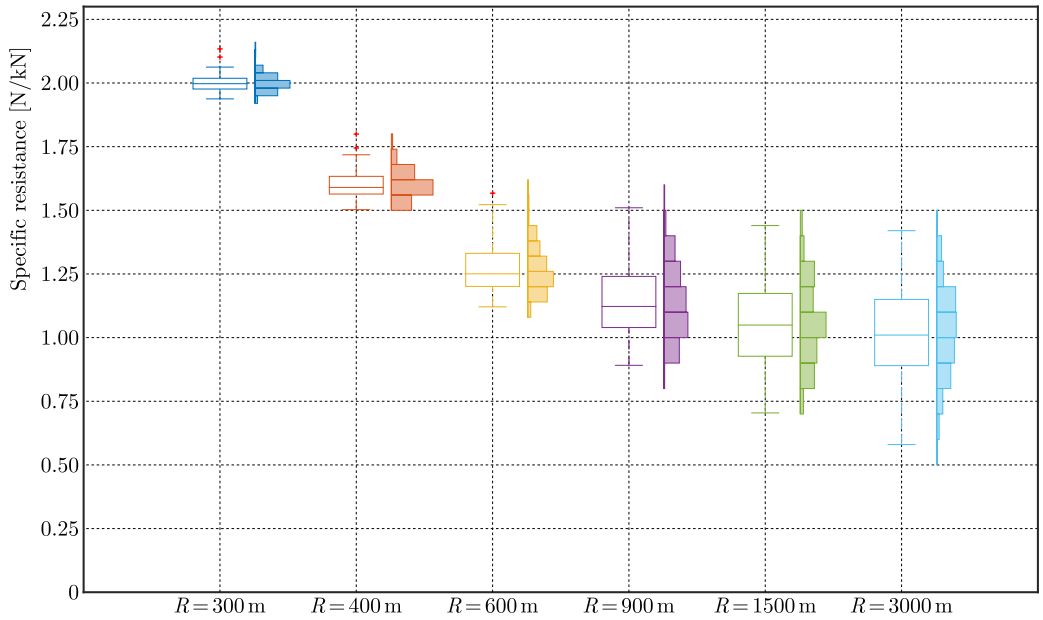

Fig. 8. Distribution of specific resistance values using boxplot and histogram, category III.

7. Conclusion

This article presents the curve resistance forces computation determined by computer-based simulation from the wheel-rail contact of a 4-axle railway vehicle moving at a constant speed on track sections with different curve radii and quality. Based on a total of more than 900 simulation results, the conclusions can be summarised as follows:

- effect of curve radius on expected curve resistance: the simulation reveals a decreasing trend in the expected curve resistance value as the track curve radius increases;
- expected curve resistance and track quality: the expected curve resistance value can be determined from the computer simulation of a stochastic dynamic process dependent on the track quality. This aligns with previous findings in the literature and highlights the sensitivity of wheel-rail contact forces against track irregularities;
- decreasing dependency with deteriorating track quality: the effect of track quality on curve resistance becomes less significant as the curve radius decreases, because the lateral movement of the vehicle is more likely determined by the geometry of the smaller radius curve;
- standard deviation and track condition: the poorer track quality, the higher the standard deviation of curve resistance, indicating larger range of the wheel-rail contact force changes;

In practice, the curve resistance forces are described by the closed-form expression, e.g., Schramm's expression. It is recommended to take into account the phenomena observed during the simulation by modifying the formulas used in practice. Different expressions can be used to describe the effect of track quality on forces of curve resistance.

A research direction could be to define a regression curve reflecting different track qualities, that can be practically useful. Further subject of research is deeper exploration of the revealed reasons for the smaller standard deviation of curve resistance at smaller track radii values and investigation of speed-dependent trends in conjunction with track superelevation to analyse their combined impact on resistance forces.

References

1. Bailey, J.R., & Hedrick, J.K. (1988). Rail vehicle energy dissipation due to lateral vehicle/track interactions. *Vehicle System Dynamics*, *17*(sup 1), 29–40. https://doi.org/10.1080/00423118808969238

2. Danz, A. (2024). boxplotGroup. *MATLAB Central File Exchange*. Retrieved December 10, 2024, from https://www.mathworks.com/matlabcentral/fileexchange/74437-boxplotgroup
3. EN 13848 standard family, *Railway applications – Track – Track geometry quality*, Part 1 2019, Part 2 2020, Part 3 2021, Part 4 2011, Part 5 2017, Part 6 2014, *European Standard*.
4. Frederich, F. (1984). Effect of track geometry on vehicle performance (in German). *ZEV-Glasers Annalen*, 12, 355–362.
5. Garg, V.K., & Dukkipati, R.V. (1984). *Dynamics of railway vehicle systems* (pp. 343–362). Elsevier. https://doi.org/10.1016/B978-0-12-275950-5.50014-6
6. Iwnicki, S.D., Stichel, S., Orlova, A., & Hecht, M. (2015). Dynamics of railway freight vehicles. *Vehicle System Dynamics*, *53*(7), 995–1033. https://doi.org/10.1080/00423114.2015.1037773
7. Jerrelind, J., Allen, P., Gruber, P., Berg, M., & Drugge, L. (2021). Contributions of vehicle dynamics to the energy efficient operation of road and rail vehicles. *Vehicle System Dynamics*, 59(7), 1114–1147. https://doi.org/10.1080/00423114.2021.1913194
8. Lukaszewicz, P. (2008). Running resistance and energy consumption of ore trains in Sweden. *Proceedings of the Institution of Mechanical Engineers, Part F: Journal of Rail and Rapid Transit*, 223(2), 189–197. https://doi.org/10.1243/09544097JRRT233
9. M. Szűcs, M., & Zábori, Z. (2024). Investigation of resistance forces from the wheel-rail interface of a four-axle railway vehicle in straight and curved track (in Hungarian). In *XIV. International Conference on Transport Sciences Győr*, 687–697.
10. Michálek, T., Kohout, M., Šlapák, J., Vágner, J., & Pulda, J. (2024). Curving and running resistance of freight trains: current experience with on-track measurements. *Vehicle System Dynamics*, 1–15. https://doi.org/10.1080/00423114.2024.2398003
11. Schmidt, E.C. (1927). Freight train curve resistance on a one-degree curve and on a three-degree curve. *University of Illinois Engineering Experiment Station*, *24*(45), Bulletin No. 167.
12. Schramm, G. (1963). Curve resistance. *Monthly Bulletin of the International Railway Congress Association*, *40*(7), 483–491.
13. Semenov, S., Mikhailov, E., Kovtanets, M., Sergienko, O., Dižo, J., Blatnický, M., Gerlici, J., & Kostrzewski, M. (2023). Kinematic running resistance of an urban rail vehicle undercarriage: a study of the impact of wheel design. *Scientific Reports*, *13*, Article 10856. https://doi.org/10.1038/s41598-023-37640-w
14. Szabó, A., Sostarics, G. & Zobory, I. (1994). Optimum axle-box guidance stiffnesses for traditional running gears operating on a given railway line. *International Journal of Vehicle Design*, 15(3–5), 484–493. https://doi.org/10.1504/IJVD.1994.061877
15. Szabó, A., & Zobory, I. (1998). On deterministic and stochastic simulation of wheel and rail profile wear process, *Periodica Polytechnica Transportation Engineering*, *26*(1–2), 3–17.
16. Tkachenko, V.P., Sapronova, S.Y., Maliuk, S.V., & Kulbovskyi, I.I. (2016). Studying the structure of railway rolling stock resistance. *Metallurgical and Mining Industry*, *11*, 30–36.
17. Tunna, J., & Urban, C. (2009). A parametric study of the effects of freight vehicles on rolling contact fatigue of rail. *Proceedings of the Institution of Mechanical Engineers, Part F: Journal of Rail and Rapid Transit*, 223(2), 141–151. https://doi.org/10.1243/09544097JRRT228
18. Wu, Q., Wang, B., Spiryagin, M., & Cole, C. (2020). Curving resistance from wheel-rail interface. *Vehicle System Dynamics*, *60*(3), 1018–1036. https://doi.org/10.1080/00423114.2020.1843689
19. Zobory, I. (1997). Prediction of wheel/rail profile wear. *Vehicle System Dynamics*, *28*(2–3), 221–259. https://doi.org/10.1080/00423119708969355
20. Zobory, I. (2008). On stochastic field model of the wheel/rail rolling/sliding contact force transfer. In *Proceedings of the 10th Mini Conference on Vehicle System Dynamics, Identification and Anomalies*, 95–116. Budapest University of Technology and Economics, Budapest, Hungary.

Manuscript received December 15, 2024; accepted for publication May 7, 2025; published online July 12, 2025.